Yiping Shao
State Key Lab of Mechanical System and Vibration;
School of Mechanical Engineering,
Shanghai Jiao Tong University,
No. 800 Dongchuan Road,
Shanghai 200240, China
e-mail: syp123gh@sjtu.edu.cn

Yaxiang Yin
School of Mechanical Engineering,
Shanghai Jiao Tong University,
No. 800 Dongchuan Road,
Shanghai 200240, China
e-mail: yaxiang@sjtu.edu.cn

Shichang Du[1]
State Key Lab of Mechanical System and Vibration;
School of Mechanical Engineering,
Shanghai Jiao Tong University,
No. 800 Dongchuan Road,
Shanghai 200240, China
e-mail: lovbin@sjtu.edu.cn

Lifeng Xi
State Key Lab of Mechanical System and Vibration;
School of Mechanical Engineering,
Shanghai Jiao Tong University,
No. 800 Dongchuan Road,
Shanghai 200240, China
e-mail: lfxi@sjtu.edu.cn

A Surface Connectivity-Based Approach for Leakage Channel Prediction in Static Sealing Interface

Leakage susceptibility is significant for the functionalization of engineering products, and surface topography plays a crucial role in forming the leakage channel in static sealing interface. This paper proposes a surface connectivity-based approach to predict the leakage channel in static sealing interface. The proposed approach consists of three modules including contact surface generation, leakage parameters definition, and leakage channel prediction. A high-definition metrology (HDM) instrument is adopted to measure the three-dimensional (3D) surface. The contact surface that can be considered as the sealing interface is generated by assembling the virtual gasket surface and waviness surface. Considering the spatial connectivity, two kinds of leakage parameters including connectivity parameters and correlation parameters are proposed to describe the characteristics of the contact surface. Meantime, a novel prediction algorithm is developed to directly indicate the potential leakage channel of the surface. Experimental results demonstrate that the proposed approach is valid to be accurate and effective, which can provide valuable information for surface topography and static sealing performance.
[DOI: 10.1115/1.4043123]

Keywords: leakage channel, static seal, connectivity, surface topography

1 Introduction

Leakage is always a serious concern, and it may lead to major security incidents and huge economic losses. In industry, leakage is one of the critical factors and important functional behaviors in performance of product quality. Seals are widely used to achieve leakage prevention, which play a role to bridge the gap between hard material components [1]. Static seal and dynamic seal are the main two forms of sealing. Static seal is simply squeezing two rough surface against each other, which is common and important in engineering applications such as the assembling interface of flanges in pipeline construction process and the joint face between engine heads and blocks in automotive powertrain manufacturing. However, in many engineering applications, leakage failure still appears even though the sealing performance is good. Therefore, modeling and diagnosing the leakage in the static sealing interface are essential to ensure the high product quality and to reduce the losses.

Research on leakage can be divided into three phases: determining whether leakage will occur, finding the leakage channel, and calculating the leak rate. Over the past few decades, numerous theoretical researches and experimental investigations have focused on this problem. From a theoretical point of view, Lebeck [2] proposed the "waviness theory," which considered the waviness effect of the end face as the reason for leakage of sealing interface in the early days. In recent years, Robbe-Valloire and Prat [3] proposed a waviness moifs-based model to analyze the surface and to calculate the leak rate. A critical junction theory had been proposed by Persson et al. who estimated the leak rate of static seals [4–6]. As an extension of Persson's method, Bottiglione et al. [7,8] presented an improved theoretical approach to explain the leakage in flat seals by considering multiple leaking passages. Soon afterward, Lorenz and Persson [9] presented an effective-medium theory of leak rates in rubber seals to further estimate the leakage mechanism. Pérez-Ràfols et al. [10] proposed a numerical model to calculate the leakage on metallic seals. Concerning experimental researches, Marie et al. first explained fluid leakage through a rough metal contact from the experimental results, and the intermediate surface component waviness was proved to be of major concern for leakage [11,12]. Lorenz and Persson [13,14] found that the leak rate of the seal is strongly dependent on the skewness of the height probability distribution of rough sealing surfaces by a series of experimental investigations. Vlădescu et al. [15] described a new apparatus to simulate a compliant sealing interface and characterized the impact of contact pressure, roughness, and surface energy on the liquid leakage.

Based on these researches, it can be concluded that leakage in static sealing interface varies as a function of contact pressure, sealing element, and surface topography. In addition, previous studies mainly reported the influences of contact pressure and sealing element. Due to the complication and variability of surface topography, it is difficult to fully control the surface topography during machining processes. Moreover, the interface topography after the assembly is not directly measurable for the limit of measurement technology. Therefore, the performance of surface topography on leakage in static seal is still at the beginning. Malburg [16] first proposed a profile filtering-based method to reveal the influences of the two-dimensional surface topography on leakage. Liao et al. [17] described the relationship between waviness and sealing performance, and the potential leak paths were found from the large tooling marks. Jianjun et al. developed a leakage channel model from the point of asperity contact of sealing interface [18]. Zhang

[1]Corresponding author.

Contributed by the Tribology Division of ASME for publication in the JOURNAL OF TRIBOLOGY. Manuscript received November 5, 2018; final manuscript received March 4, 2019; published online March 25, 2019. Assoc. Editor: Joichi Sugimura.

et al. [19] described an approach to calculate the leak channel and leak rates between metallic sealing surfaces based on three-dimensional finite element contact analysis. Ren et al. [20] proposed a lattice graph model to diagnosis the potential leak areas for surface assembly. Shao et al. [21] proposed a leakage monitoring method in static sealing interface based on the three-dimensional (3D) surface topography indicator. All these studies have provided the direct evidence of a strong relationship between surface topography and leakage. However, both theoretical contact mechanics analysis and finite element analysis require approximate assumptions, which may be different from the reality. Experimental research could not reveal the multiscale effect of surface topography on leakage. More recently, Liu et al. [22] proposed a connectivity characterization method to reveal the correlation between surface topography and sealing performances, which explored the leakage from a new angle of view. But the definition of connectivity index was incomprehensive, and the mechanism that surface connectivity influenced on the leakage was not explained. Meanwhile, to the best knowledge of the authors, there is a significant lack of research that evaluates the surface connectivity. Therefore, surface topography is still the focus of researches for leakage and sealing performance, and surface connectivity can be accepted as a new research approach to reflect the leakage channel. Therefore, the limitations of current methods are summarized as follows:

- Most theoretical studies that contain contact mechanics analysis and finite element analysis are based on simplified assumptions, and they have not provided the actual entire surface topography with the lack of appropriate measurement instrument.
- Due to the existence of multiscale surface, the experimental research could not reveal the multiscale effect of surface topography on leakage.
- The spatial distribution and surface connectivity of the sealing interface, which are related to leakage channel, have rarely been considered in previous studies, and the effect of the surface connectivity on leakage channel is not clear.

In recent years, precision measurement technology has shown a rapid development trend. A recently developed noncontact measurement instrument named high-definition metrology (HDM) are adopted in this paper [23]. It can generate millions of data points within seconds to represent the entire 3D surface topography. The measurement resolution is 150 μm in x–y-direction and 1 μm in z-direction, respectively. The HDM device and an example of the HDM-measured engine block face are shown in Fig. 1. Benefitting from the high precision and full measurement, a large number of studies on the 3D surface topography have been developed to make a thorough understanding of the manufacturing process [24–30].

With the novel measurement platform, the main contribution of this paper is to propose a novel surface connectivity-based approach to predict the potential leakage channel through surface topography. First, a recently proposed approach in our previous research [21] is adopted to generate the contact surface, which can be considered as the sealing interface. The contact surface is defined by assembling the virtual gasket surface and waviness surface. Then, considering the spatial connectivity, two kinds of leakage parameters including connectivity parameters and correlation parameters are proposed to describe the characteristics of the contact surface. Finally, a novel prediction algorithm is developed to directly indicate the potential leakage channel of the surface.

The remainder of this paper is organized as follows. A brief introduction of the connectivity is recalled in Sec. 2. In Sec. 3, the leakage channel prediction approach is described in detail. Case studies demonstrate the effectiveness of the proposed method in Sec. 4. Section 5 concludes this study.

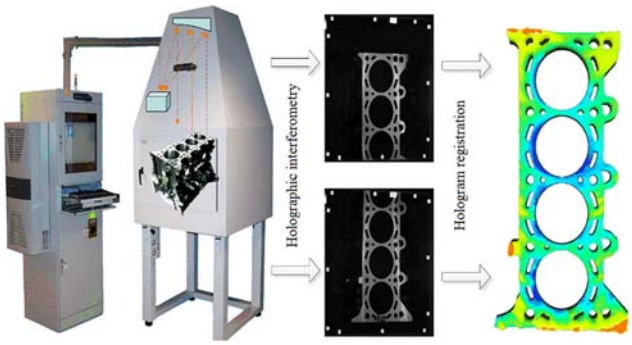

Fig. 1 Measurement by HDM

2 Brief Introduction of Connectivity

The mathematical notion of connectivity is widely used in the topological framework and the graph-theoretic framework [31]. The classical connectivity plays an important role in image processing and analysis, and it has been extensively used in different fields. To overcome the incompatibility between the topological connectivity and the graph-theoretic connectivity, Serra [32] proposed a formal definition of connectivity class in a complete lattice framework based on the mathematical morphology. Here, some basic theoretical concepts are recalled and explained as follows.

(1) Connectivity class

Definition. Let Z be a set of points and X be a subset of Z. For two arbitrary points $a, b \in X$, there exists a continuous mapping ϕ from [0, 1] into X, which satisfies $\phi(0) = a$ and $\phi(1) = b$, and then X is a connectivity class. Hence, the continuous mapping ϕ can be a path from a to b and belonging completely into X.

In the definition, the continuous mapping ϕ depends on the connection of adjacent points. Therefore, the adjacency principle between neighboring points will directly affect the form of connectivity class.

(2) Adjacency principle

Suppose that a set X is a connectivity class, which can be 4-connected or 8-connected depending on the 4-adjacency (d_4) and 8-adjacency (d_8) principles. The two principles describe the different definitions of distance, which are defined as follows:

$$d_4 = |x_1 - x_2| + |y_1 - y_2| \tag{1}$$

$$d_8 = \max\{|x_1 - x_2|, |y_1 - y_2|\} \tag{2}$$

where (x_1, y_1) and (x_2, y_2) are two arbitrary points in X. Figure 2 shows three different points: $a(2, 3)$, $b(3, 3)$, and $c(3, 2)$. Based on Eq. (1), $d_4(a, b) = 1$ and $d_4(a, c) = 2$, where a, b are neighboring points and a, c are not neighboring points. But based on Eq. (2), $d_8(a, b) = d_8(a, c) = 1$ and both a, b and a, c are neighboring points.

According to 4-adjacency (d_4) principle, an example of connectivity class are given in Fig. 3. Two sets X_1 and X_2 are made up of several points, and X_{21} and X_{22} are two subsets of X_2. Then,

$$X_1 = \{(1, 4), (1, 3), (2, 2), (2, 3), (2, 4), (3, 1), (3, 2), (3, 3)\} \tag{3}$$

$$X_2 = \{(1, 4), (1, 3), (2, 2), (2, 4), (3, 1), (3, 2), (3, 3)\} \tag{4}$$

$$X_{21} = \{(1, 4), (1, 3), (2, 4)\} \tag{5}$$

$$X_{22} = \{(2, 2), (3, 1), (3, 2), (3, 3)\} \tag{6}$$

Based on the definition of connectivity class, the continuous mapping ϕ is a path between two arbitrary points using 4-adjacency principle. It is clear that there always exists a path between two arbitrary points in X_1, but it cannot meet the condition in X_2. Therefore, X_1 is a connectivity class and X_2 is not a connectivity class. Both subsets X_{21} and X_{22} are connectivity classes. Here, in this paper, 4-adjacency principle is employed, and the continuous mapping ϕ

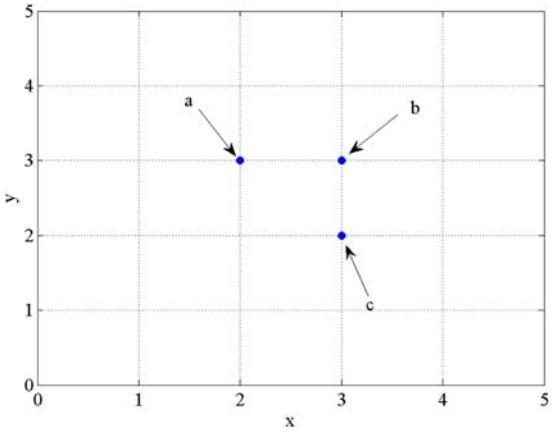

Fig. 2 Examples of different adjacency principles

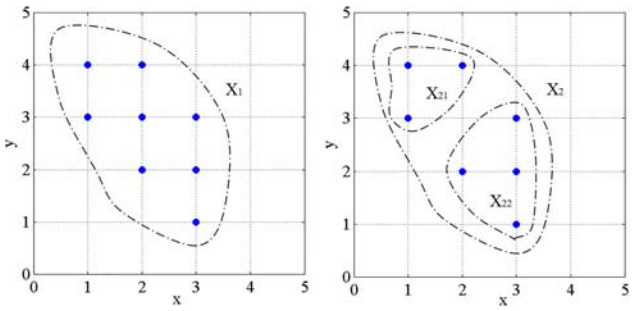

Fig. 3 Examples of connectivity class

is considered as a path between two arbitrary points.

(3) Lattice operators

Lattice operators play an essential role to realize the measure of connectivity. In the complete lattice framework, there are four basic lattice operators including dilation, erosion, opening, and closing. They are defined as follows:

Dilation:

$$\delta_B(X) = X \oplus B \tag{7}$$

Erosion:

$$\varepsilon_B(X) = X \ominus B \tag{8}$$

Opening:

$$\gamma_B(X) = X \circ B = \delta_B(\varepsilon_B(X)) = (X \ominus B) \oplus B \tag{9}$$

Closing:

$$\beta_B(X) = X \bullet B = \varepsilon_B(\delta_B(X)) = (X \oplus B) \ominus B \tag{10}$$

where X is the input connectivity class, B is the compact convex structuring element, and $\oplus$ and $\ominus$ denote the Minkowski addition and subtraction, respectively. Here, spherical structuring element is adopted in this paper.

(4) Multiscale operators

To quantify the degree of connectivity, lattice operators are extended into multiscale lattice operators. The structuring element B is replaced by a multiscale version rB. Here, $rB = \{rb : b \in B,\ r \geq 0\}$. Therefore, the multiscale dilation, multiscale erosion, multiscale opening, and multiscale closing can be recursively defined as follows:

Multiscale dilation:

$$\delta_B^r(X) = X \oplus rB = \delta_B(\delta_B^{r-1}(X)) = \cdots = \delta_B(\delta_B \ldots \delta_B(\delta_B(X))) \tag{11}$$

Multiscale erosion:

$$\varepsilon_B^r(X) = X \ominus rB = \varepsilon_B(\varepsilon_B^{r-1}(X)) = \cdots = \varepsilon_B(\varepsilon_B \ldots \varepsilon_B(\varepsilon_B(X))) \tag{12}$$

Multiscale opening:

$$\gamma_B^r(X) = X \circ rB = \delta_B^r(\varepsilon_B^r(X)) \tag{13}$$

Multiscale closing:

$$\beta_B^r(X) = X \bullet rB = \varepsilon_B^r(\delta_B^r(X)) \tag{14}$$

where $\delta_B^0(X) = X$, $\varepsilon_B^0(X) = X$, and $r = 1, 2, 3\ldots$, $r \in \mathbb{N}_+$.

(5) Conditional operators

Since the dilation operator is extensible, the original connectivity class X will exceed the boundary when the dilation is repeatedly performed without restriction. The way to avoid this problem is to limit the dilation operator in a specific mask. Therefore, a new nontranslational invariance dilation operator named conditional dilation is defined as follows:

$$\delta_B(X|Y) = (X \oplus B) \cap Y \tag{15}$$

where Y is a mask of X.

3 The Proposed Method

This section describes an overview of the proposed approach, which consists of three modules including contact surface generation, leakage parameters definition, and leakage channel prediction. The framework of the proposed approach is shown in Fig. 4. In module 1, the contact surface is defined by assembling the virtual gasket surface and waviness surface. A recently proposed approach by Shao et al. [21] is adopted to generate the contact surface, which reflects leakage. In module 2, two kinds of leakage parameters including connectivity parameters and correlation parameters are proposed to describe the characteristics of the contact surface. In module 3, a novel leakage channel prediction algorithm is developed based on the proposed leakage parameters. A leakage index Ψ is built to directly indicate the potential leakage channel of the surface. The procedure of module 1 is described in detail in Sec. 3.1, whereas the procedure of modules 2 and 3 are elaborated in Secs. 3.2 and 3.3, respectively.

3.1 Contact Surface Generation. Based on the conclusions in Refs. [12,16,21], the intermediate surface component waviness was the major factor on leakage. Therefore, a recently proposed approach in our previous research [21] is adopted to generate the contact surface, which reflects the potential leakage channel. The contact surface is generated by assembling the virtual gasket surface and waviness surface. A flowchart of the approach is shown in Fig. 5, and the detailed procedures are described as follows:

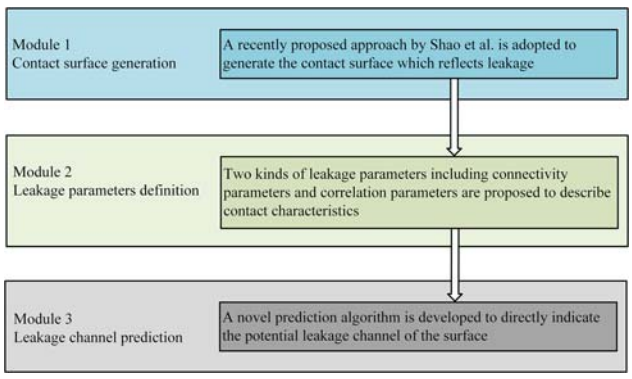

Fig. 4 The framework of the proposed method

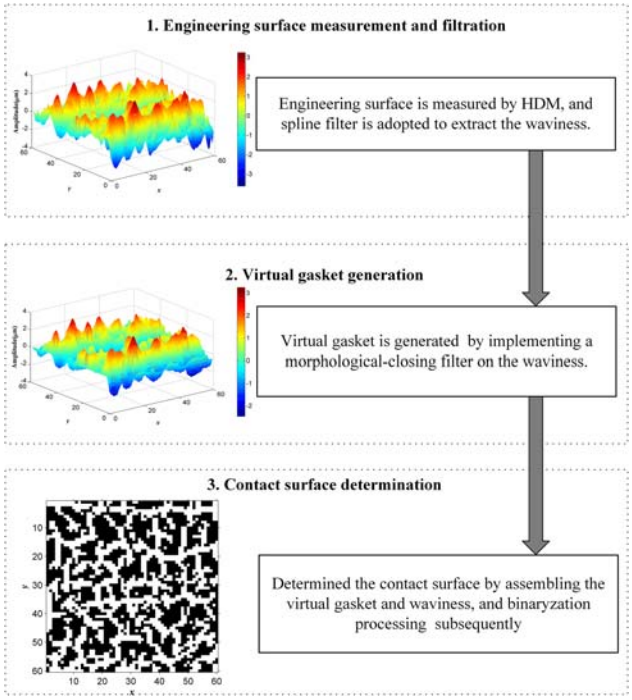

Fig. 5 The architecture of the contact surface generation approach

Step 1: Engineering surface measurement and filtration

With the precision measurement platform, the entire and accuracy engineering surface data are measured by HDM. It is noted that the measured HDM data do not contain the three-dimensional roughness information with the limitation of the resolution in z-direction. For example, Fig. 6 shows the measured results of engine cylinder head and block surfaces.

In surface metrology, surface filtration is mainly adopted to clarify the effect mechanism of different surface components [33]. Spline filter is a widely used linear filter that has been described clearly in ISO 16610-22 [34]. Two-dimensional surface components can be separated exactly from large scale to small scale by a profile spline filter. With the continuous improvement of ISO 16610, spline filter has been proposed to separate the three-dimensional surface components, which is planned to be published in ISO 16610-62. Therefore, the waviness can be separated from the original high-resolution measured surfaces exactly, and Fig. 7 shows a clear illustration.

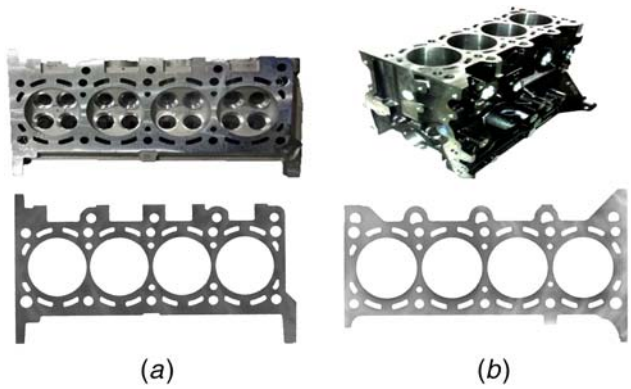

Fig. 6 (*a*) Engine cylinder head surface and (*b*) engine cylinder block surface

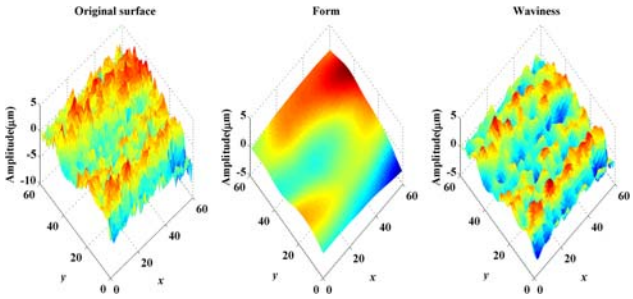

Fig. 7 Filtered results of an areal spline filter

Step 2: Virtual gasket generation

Gasket seal is a main sealing form in many engineering products that require high security seals. As mentioned earlier, the actual topography information and deformation of the assembled gasket are not directly measurable in practice. As an attempt, a novel concept called virtual gasket is proposed in our previous research, which is used to achieve the simulation of contact [21]. In the geometrical product specification, a morphological filter is usually employed to reflect the geometrical features of engineering surfaces [35]. Therefore, the virtual gasket is generated by implementing a morphological closing filter on the latest filtered waviness. For example, a virtual gasket profile and a virtual gasket surface are shown in Fig. 8.

Step 3: Contact surface determination

When both the waviness $SW(x, y)$ and virtual gasket $SC(x, y)$ are obtained, the final step is to generate the contact surface. In the reference of [21], three areal leakage parameters such as CAP (contact area percentage), VV (void volume), and $SWvoid$ (relative void volume) are proposed as indicators that report whether the leakage has occurred. A brief review is described as follows. The three areal leakage parameters are defined as follows:

$$CAP = \sum_{S} [\text{if } (SC_i(x, y) = SW_i(x, y))1 \text{ else } 0]/S \tag{16}$$

$$VV = \iint_{S} (SC(x, y) - SW(x, y))dxdy \tag{17}$$

$$SWvoid = VV/S \tag{18}$$

where S denotes the nominal area of the surface. Due to the independence of $SWvoid$, it is validated to monitor leakage. When the leakage parameter $SWvoid$ in a surface is greater than the threshold $SWvc$, this surface is called a leakage surface. Therefore, once the leakage surface is found, it is necessary to clarify the leakage channel further. It is clear that the contact condition between the virtual gasket and the waviness is closely related to the leakage channel. Let Z be the contact surface, which is generated by assembling the virtual gasket and waviness. Depending on whether the two surfaces contact, the contact surface Z can be considered as a binary image. Then, it can be defined as follows:

$$Z = \begin{cases} 0 & SC(x, y) \le SW(x, y) \quad \text{contact} \\ 1 & SC(x, y) > SW(x, y) \quad \text{no contact} \end{cases} \tag{19}$$

where $Z = 0$ means total contact and $Z = 1$ means no contact. $SW(x, y)$ and $SC(x, y)$ denote the value in z-direction of the waviness surface and the virtual gasket surface, respectively, which represent the surface height information.

It is noted that the calculation of the contact surface is based on comparing the value of the virtual gasket surface and waviness surface in z-direction. The surface

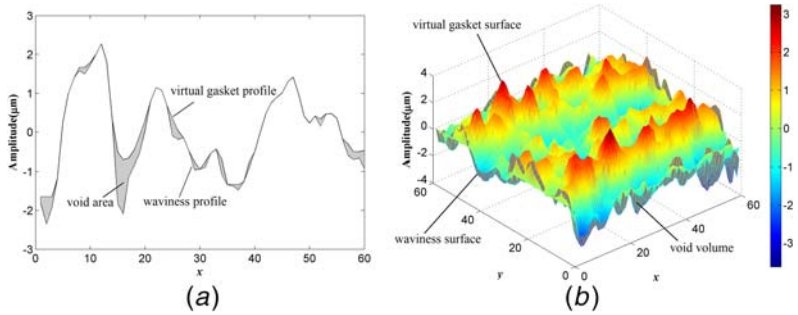

Fig. 8 (*a*) Virtual gasket profile and (*b*) virtual gasket surface

height information of both the virtual gasket surface and waviness surface obey random distribution. According to the knowledge of probability and statistics theory, the size of sampling areas will not affect the surface height distribution. Meantime, when two surfaces are in contact, the percentage of the contact area at a given average normal pressure is independent with the system size for a fixed surface [36], but the amount of the surface data and computational efficiency depend on the size of sampling areas. Therefore, the size of sampling area has no influence on the distribution of the contact surface but has influence on the calculation time of the contact surface, and the size of sampling area can be selected by engineering practice.

Based on the above procedures, a typical illustration of the contact surface is shown in Fig. 9. It can be seen that each square of the lattice, which represents the contact area, is either black or white. (The black denotes total contact, and the white denotes no contact.) The contact surface is actually a binary image that does not contain height information, and all the next processes are based on the contact surface.

3.2 Leakage Parameters Definition. After obtaining the contact surface, the next process is to focus on the descriptions of contact characteristics, which is related to the leakage channel. Connectivity is a concept from topological geometrical theory, and the connectivity of the contact surface plays an important role in lubrication, surface distribution, and sealing performance [20,22,37]. The connectivity varies from surface to surface, even if the surfaces have same amplitude parameters. To the best knowledge of the authors, there is a significant lack of research that evaluates the surface connectivity. Up to now, there is no specific standard or systematic evaluation method for surface connectivity. Therefore, a series of leakage parameters based on the connectivity are defined in this subsection. The proposed leakage parameters can be divided into two categories: connectivity parameters and correlation parameters. Connectivity parameters are defined to evaluate the connectivity measure of a single connectivity class, and correlation parameters used to indicate the correlation among multiple connectivity classes.

3.2.1 Connectivity Parameters. In general, the contact surface Z is represented by a matrix consisting of a set of discrete points in discrete spaces. Therefore, the concept of connectivity is actually a geometrical relationship between these discrete points.

As shown in Fig. 9, there are more than one connectivity class, which have different shapes and sizes in the surface Z. For each connectivity class, there always exists a narrowest path that can be regarded as the weakest place of the connectivity class. Some other typical examples are shown in Fig. 10. A_1, A_2, and A_3 are three different connectivity classes, and the size of these connectivity classes satisfies $\mu(A_1) > \mu(A_2) > \mu(A_3)$ with the condition of $R_1 > R_2$ and $h_1 > h_2$. To distinguish these connectivity classes, the connectivity measure of a single connectivity class is necessary. In other words, the connectivity measure is to evaluate the narrowest path.

Several connectivity measure methods including multiresolution connectivity measure, generalized connectivity measure, erosion-based connectivity measure, and adjunctional connectivity measure have been described by Tzafestas and Maragos [31]. As a similar extension, an extended operator called multiscale conditional operator and a modified connectivity measure called average adjunctive multiscale connectivity function $\bar{\mu}_\alpha$ are developed based on Tzafestas' conclusions in this paper. Suppose X is one part of Z and X is a connectivity class. The definitions of the two parameters are given as follows.

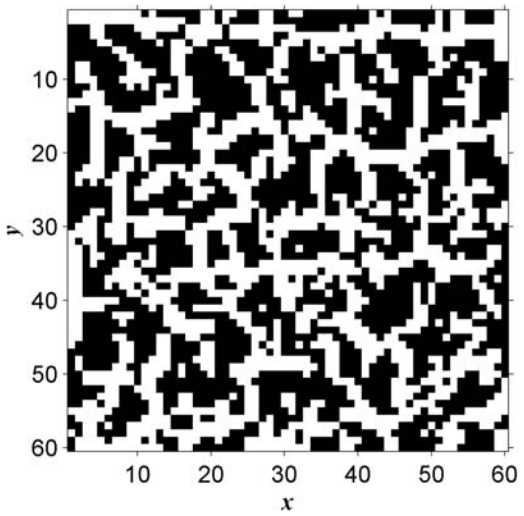

Fig. 9 Contact surface

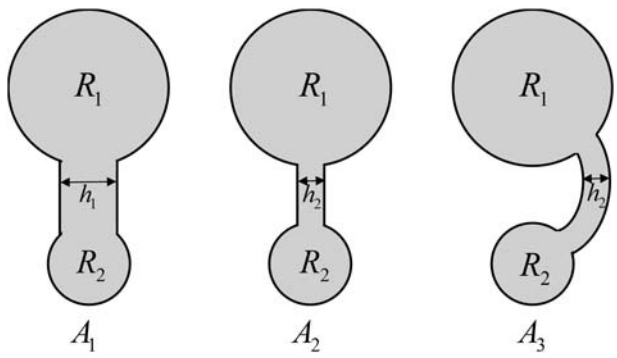

Fig. 10 Different connectivity classes

(1) Multiscale conditional operators

Following the logic of multiscale operators, the multiscale conditional dilation can be defined as

$$\delta_B^r(X|Y)=\delta_B(\delta_B^{r-1}(X|Y)|Y)=\cdots=\delta_B(\delta_B(\ldots\delta_B(\delta_B(X|Y)|Y)\ldots|Y)|Y) \tag{20}$$

where X is the connectivity class and Y is a mask of X. B is a compact convex structuring element and r is the scale $r=1, 2, 3\ldots, r\in\mathbb{N}_+$. In this way, both the length and the width of the narrowest path within the connectivity class are considered.

(2) Average adjunctive multiscale connectivity function

Suppose $\alpha=(\varepsilon_B, \delta_B)$ is an adjunction on $P(E)$. The adjunctive multiscale connectivity function μ_α is defined as

$$\mu_\alpha(X, s)=\exp(-\lambda r_\alpha(X, s)) \tag{21}$$

where $r_\alpha(X, s)=inf\{r\in\mathbb{N}_+:\delta_B^r(\varepsilon_B^s(X)|X)=1\}$, and $\lambda>0$ is a parameter that denotes the rate of exponential function. λ is not a fixed value that is used to adjust the slope of the function, and it is different in various applications. According to the previous research and practice [31], $\lambda=0.05$ is suitable in this paper. $s\in[0, s_{\max}]$ is the scale, and $s_{\max}$ denotes the maximum applicable scale, which is defined as follows:

$$s_{\max}=\{s_{\max}\in\mathbb{N}_+:n(\varepsilon_B^{s_{\max}}(X))=0, X\in P(E)\} \tag{22}$$

where $n(X)$ denotes the number of connectivity classes in X, E is a two dimensional linear space and $P(E)$ is the power set. Therefore, the average adjunctive multiscale connectivity function $\bar{\mu}_\alpha$ is calculated as

$$\bar{\mu}_\alpha=\frac{1}{s_{\max}}\sum_{s=0}^{s_{\max}}\mu_\alpha(X, s)\quad\bar{\mu}_\alpha\in[0, 1] \tag{23}$$

Based on the definition, the proposed connectivity function $\bar{\mu}_\alpha$ not only contains the full geometrical features (shape and size) but also integrates the multiscale information. To be specific, $\bar{\mu}_\alpha$ indicates "how slow" a connectivity class becomes disconnected or vanishes. When $\bar{\mu}_\alpha\to 0$, X is "nearly disconnected." Oppositely, when $\bar{\mu}_\alpha\to 1$, X is "completely connected." That is to say, the larger $\bar{\mu}_\alpha$ means the larger size of the connectivity class. Actually, $\bar{\mu}_\alpha$ is to evaluate the "width" and "length" of the "narrowest" path of X. For example, the three connectivity classes A_1, A_2, and A_3 have different "width" and "length" in Fig. 10. Due to the condition of $R_1>R_2$ and $h_1>h_2$, it is apparent that $\mu(A_1)>\mu(A_2)>\mu(A_3)$, which is consistent with the definition of $\bar{\mu}_\alpha$.

In a static sealing interface, leakage channel depends strongly on the geometry of contact, and the distribution of surface height has a great influence on the contact condition. At the same time, surface connectivity is an intuitive performance of the distribution of surface height. Furthermore, the size of the connectivity class reflects the leakage channel resistance (similar to conductance in electronics). Once the size of the connectivity class is lower, the flow of lubricant meets more hindrance. On the contrary, the larger the size of the connectivity class, the easier the fluid will pass through the channel, and more probably the leakage channel will appear. Therefore, the proposed connectivity function $\bar{\mu}_\alpha$ can be used to predict the leakage channel.

3.2.2 Correlation Parameters. As mentioned earlier, there are many connectivity classes in the surface Z. Once the connectivity measure of a single connectivity class is determined, it is necessary to further evaluate the correlation among multiple connectivity classes. Therefore, an attempt is made to propose three connectivity correlation parameters, which indicate the corrlation between the two arbitrary independent connectivity classes. The three correlation parameters are minimum connective distance (*mcd*), average connective distance (*acd*), and cross connectivity index θ, respectively. Note that Euclidean distance is adopted in *mcd* and *acd*. The detailed definitions of these parameters are described as follows.

(1) Minimum connective distance

Minimum connective distance (*mcd*) is the description of the minimum distance between two independent connectivity classes. Assume that X_p and X_q are two independent connectivity classes, then E^p and E^q are the corresponding edge matrices that satisfy

$$E^p=Ed(X_p) \tag{24}$$

$$E^q=Ed(X_q) \tag{25}$$

where Ed is the general edge detector. The minimum connective distance mcd_{pq} between X_p and X_q can be defined as

$$mcd_{pq}=\min|E_i^p-E_j^q|=\sqrt{(x_i^p-x_j^q)^2+(y_i^p-y_j^q)^2}\quad(i=1, 2, \ldots, mc_p, j=1, 2, \ldots, mc_q) \tag{26}$$

where mc_p is the number of E^p and mc_q is the number of E^q.

(2) Average connective distance

The average connective distance (*acd*) reflects the mean distance between two independent connectivity classes. It is defined by the center of two connectivity classes. The average connective distance acd_{pq} between X_p and X_q can be calculated as

$$acd_{pq}=\sqrt{(\bar{x}^p-\bar{x}^q)^2+(\bar{y}^p-\bar{y}^q)^2} \tag{27}$$

$$\bar{x}^p=\sum_{i=1}^{mc_p}x_i^p, \bar{y}^p=\sum_{i=1}^{mc_p}y_i^p \tag{28}$$

$$\bar{x}^q=\sum_{j=1}^{mc_q}x_j^q, \bar{y}^q=\sum_{j=1}^{mc_q}y_j^q \tag{29}$$

where $(\bar{x}^p, \bar{y}^p)$ and $(\bar{x}^q, \bar{y}^q)$ are the centers of X_p and X_q.

(3) Cross connectivity index

Cross connectivity index θ is proposed to describe the connection degree between two independent connectivity classes. It is defined by, respectively, dilating arbitrary two independent connectivity classes X_p and X_q with the same structuring element until a new connectivity class BDX_{pq} is generated. Here, we call BDX_{pq} bi-dilational connectivity class. It not only contains the original components of X_p and X_q but also the first-generated connectivity class during the dilation. Thus, the formulation of θ is described as follows:

$$BDX_{pq}=\delta_B^{\theta-1}(X_p+X_q) \tag{30}$$

$$\theta=\{\theta\in\mathbb{N}_+:n(\delta_B^\theta(X_p+X_q))=2 \text{ and } n(\delta_B^{\theta-1}(X_p+X_q))=1, X_p, X_q\in P(E)\} \tag{31}$$

where $n(X)$ denotes the number of connectivity classes in X. The proposed cross connectivity index can distinguish the strong and weak correlation between different independent connectivity classes, which directly influences the distribution of the leakage channels and the seal performances of contact surface.

3.3 Leakage Channel Prediction. Based on the proposed leakage parameters, a novel leakage channel prediction algorithm is developed. The key problem of the proposed prediction algorithm is to build a leakage index Ψ, which can directly indicate the potential leakage channel of the surface. An architecture of the developed algorithm is shown in Fig. 11, and the detailed procedures are described as follows.

Step 1: Connectivity class determination

Once the contact surface Z is generated, the first step is to find out the connectivity class X_i of the surface based on the aforementioned connectivity definition. Meanwhile, the number of connectivity classes n is determined. Here, $i=1, 2, \ldots, n$.

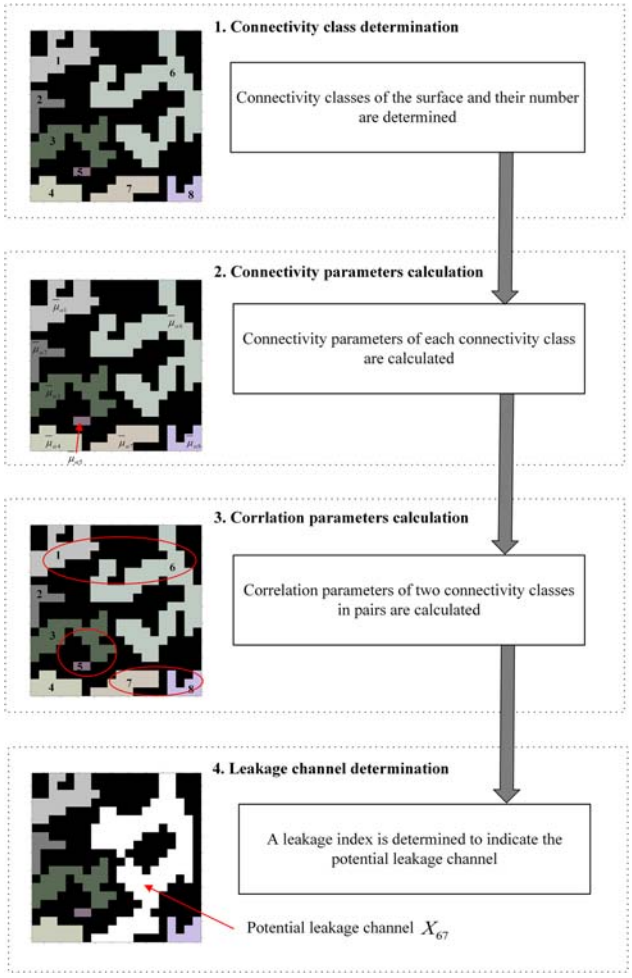

Fig. 11 The architecture of the leakage channel prediction algorithm

Step 2: Connectivity parameters calculation

As for each connectivity class, all the connectivity parameters are calculated. The average adjunctive multiscale connectivity functions $\bar{\mu}_\alpha(X_i)\,(i=1,2,\ldots,n)$ are adopted to represent the size of connectivity of the connectivity class X_i. For convenience, $\bar{\mu}_{\alpha i}=\bar{\mu}_\alpha(X_i)$.

Step 3: Correlation parameters calculation

Due to multiple connectivity classes, the correlation parameters of two connectivity classes in pairs are calculated. Let $Corr_{ij}=\{mcd_{ij}, acd_{ij}, \theta_{ij}\}$ be the integrated index of these correlation parameters including minimum connective distance, average connective distance, and cross connectivity index for connectivity classes X_i and X_j. Here, $i=1, 2, \ldots, n$, $j=1, 2, \ldots, n$, and $i\neq j$.

Step 4: Leakage channel determination

When both connectivity parameters and correlation parameters are obtained, a leakage index Ψ is proposed to indicate the potential leakage channel. The leakage index Ψ is also named as breakthrough index, which defines whether a connectivity class traverses the entire surface. In engineering practice, the flow pressure only acts in one direction, and thus, the traversed direction is considered in y-direction of the entire surface. Assume that z_{ys} and z_{ye} are the minimum and maximum coordinate values of the surface Z, respectively, and then, the breakthrough index of the connectivity class X_i is calculated as

$$\Psi(X_i)=\begin{cases}1, & \min\{y_j^i\}=z_{ys} \text{ and } \max\{y_j^i\}=z_{ye}\\ 0, & \text{else}\end{cases} \tag{32}$$

where $\min\{\cdot\}$ and $\max\{\cdot\}$ are the operations of taking the minimum and maximum values, respectively.

Obviously, there are two cases Ψ_1 and Ψ_2 in the definition of Ψ. If it satisfies $\Psi_1=1$, the entire surface is traversed. On the contrary, the entire surface is not traversed when it meets the condition of $\Psi_2=0$.

Case 1. For $\Psi_1=1$, the potential leakage channel exists prominently in the contact surface, and it must be one of the connectivity classes. To be specific, it can be described as follows:

- If it satisfies $\Psi(X_i)=1$, then the connectivity class X_i is the potential leakage channel.
- If it satisfies $\Psi(X_j)=1$, then the connectivity class X_j is the potential leakage channel.

Case 2. For $\Psi_2=0$, it does not exist the significant condition that a single connectivity class can be considered as a potential leakage channel. Then, the correlation and the size of connectivity is used to indicate the potential leakage channel.

First, a new concept called bi-closing connectivity class is defined as

$$X_{pq}=\beta_B^h(X_p+X_q) \tag{33}$$

where $h=\{h\in\mathbb{N}_+ : n(\beta_B^h(X_p+X_q))=1\}$ is the specific applicable scale. The bi-closing connectivity class is defined by respectively closing arbitrary two independent connectivity classes X_p and X_q with the same structuring element until a new connectivity class X_{pq} is generated. Different from the bi-dilational connectivity class X_{pq}, the bi-closing connectivity class X_{pq} would not exceed the boundary when the operator is repeatedly performed. It well inherits the nature of the original connectivity classes and has revealed the information about potential leakage channel.

Second, calculating all the average adjunctive multiscale connectivity functions $\bar{\mu}_{\alpha i}$ of each connectivity class, the maximum $\bar{\mu}_\alpha(X_{k_0})=\max\{\bar{\mu}_{\alpha i}|i=1,2,\ldots,n\}$ of the connectivity class X_{k_0} is found.

Third, all the correlation parameters $Corr_{ij}$ of two connectivity classes in pairs are compared. The minimum value of three parameters including minimum connective distance, average connective distance, and cross connectivity index are found as follows:

$$mcd_{k_1k_2}=\min\{mcd_{ij}|i=1,2,\ldots n, j=1,2,\ldots n, i\neq j\} \tag{34}$$

$$acd_{k_3k_4}=\min\{acd_{ij}|i=1,2,\ldots n, j=1,2,\ldots n, i\neq j\} \tag{35}$$

$$\theta_{k_5k_6}=\min\{\theta_{ij}|i=1,2,\ldots n, j=1,2,\ldots n, i\neq j\} \tag{36}$$

Next, the average adjunctive multiscale connectivity functions $\bar{\mu}_\alpha(X_{k_1k_2})$, $\bar{\mu}_\alpha(X_{k_3k_4})$, and $\bar{\mu}_\alpha(X_{k_5k_6})$ of bi-closing connectivity classes $X_{k_1k_2}$, $X_{k_3k_4}$, and $X_{k_5k_6}$ are calculated. Here, k_0, k_1, k_2, k_3, k_4, k_5, and $k_6\in\{1,2,\ldots,n\}$ denote the corresponding connectivity class.

Finally, the values among $\bar{\mu}_\alpha(X_{k_0})$, $\bar{\mu}_\alpha(X_{k_1k_2})$, $\bar{\mu}_\alpha(X_{k_3k_4})$, and $\bar{\mu}_\alpha(X_{k_5k_6})$ are compared, and the maximum $\bar{\mu}_\alpha(X_k)$ is found, which is defined as

$$\bar{\mu}_\alpha(X_k)=\max\{\bar{\mu}_\alpha(X_{k_0}),\ \bar{\mu}_\alpha(X_{k_1k_2}),\ \bar{\mu}_\alpha(X_{k_3k_4}),\ \bar{\mu}_\alpha(X_{k_5k_6})\} \tag{37}$$

where the subscript $k\in\{k_0, k_1k_2, k_3k_4, k_5k_6\}$. Therefore, the connectivity class or bi-closing connectivity class X_k is considered as the potential leakage channel.

Analogously, all the leakage parameters are calculated on the contact surface, and the surface connectivity is only affected by the distribution of the contact surface. As mentioned earlier, the size of sampling area has no influence on the distribution of the contact surface but has influence on the calculation time of the contact surface. Therefore, the size of sampling area will not affect the surface connectivity, and it can be selected by engineering practice.

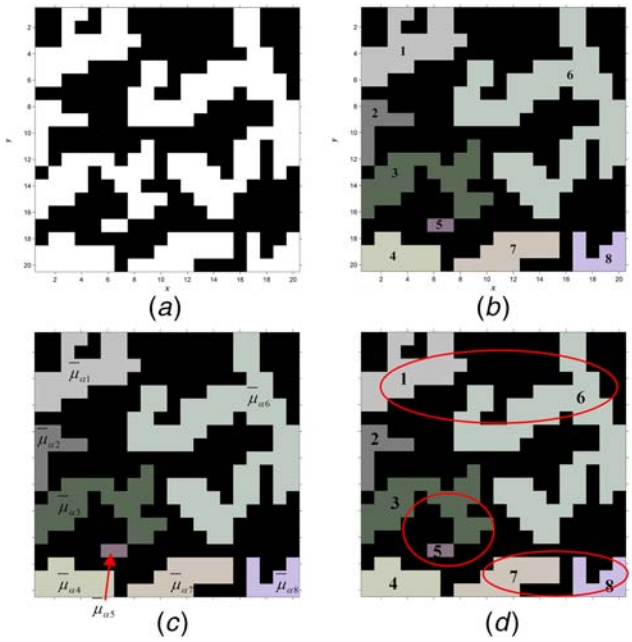

Fig. 12 (a) A 20 × 20 contact surface *Z*, (b) different connectivity classes, (c) connectivity parameters $\bar{\mu}_{\alpha i}$, and (d) correlation parameters $Corr_{ij}$

Example 1. Considering the computational efficiency, a 20×20 contact surface Z is shown in Fig. 12(*a*). In Fig. 12(*b*), the connectivity classes are marked in different grayscales, and the number of connectivity classes is $n = 8$. Here, the grayscales do not mean the height information but mean different connectivity classes.

Subsequently, connectivity parameters $\bar{\mu}_{\alpha i} (i = 1, 2, \ldots, 8)$ and correlation parameters $Corr_{ij} (i = 1, 2, \ldots, 8, j = 1, 2, \ldots, 8,$ and $i \neq j)$ are calculated, which are shown in Figs. 12(*c*) and 12(*d*). The detailed results are summarized in Tables 1 and 2.

Obviously, all the values of Ψ are equal to 0, and it satisfies the case $\Psi_2 = 0$, and the results are obtained as follows:

$$\begin{cases} \bar{\mu}_{\alpha k_0} = \bar{\mu}_{\alpha 6} = 1.168 \\ mcd_{k_1 k_2} = \{mcd_{17}, mcd_{18}, mcd_{25}, mcd_{35}, mcd_{46}, mcd_{78}\} = 1.41 \\ acd_{k_3 k_4} = \{acd_{45}\} = 3.61 \\ \theta_{k_5 k_6} = \{\theta_{12}, \theta_{16}, \theta_{23}, \theta_{34}, \theta_{35}, \theta_{36}, \theta_{45}, \theta_{47}, \theta_{67}, \theta_{78}\} = 1 \end{cases} \tag{38}$$

The maximum value of connectivity $\bar{\mu}_\alpha(X_k)$ is calculated as

$$\bar{\mu}_\alpha(X_k) = \max \begin{Bmatrix} \bar{\mu}_\alpha(X_6), \bar{\mu}_\alpha(X_{17}), \bar{\mu}_\alpha(X_{18}), \bar{\mu}_\alpha(X_{25}), \bar{\mu}_\alpha(X_{35}), \bar{\mu}_\alpha(X_{46}), \\ \bar{\mu}_\alpha(X_{78}), \bar{\mu}_\alpha(X_{45}), \bar{\mu}_\alpha(X_{12}), \bar{\mu}_\alpha(X_{16}), \bar{\mu}_\alpha(X_{23}), \bar{\mu}_\alpha(X_{34}), \\ \bar{\mu}_\alpha(X_{35}), \bar{\mu}_\alpha(X_{36}), \bar{\mu}_\alpha(X_{47}), \bar{\mu}_\alpha(X_{67}) \end{Bmatrix} = \bar{\mu}_\alpha(X_{67}) = 1.174 \tag{39}$$

Hence, the bi-closing connectivity class X_{67} is considered as the potential leakage channel, which is shown in Fig. 13.

4 Case Study

In vehicle powertrain, leakage is always an important issue. Especially, leakage in an internal combustion engine can result in compression loss, power reduction, and engine overheating. To demonstrate the ability of the proposed methodology for engineering practice, a case study on the interface between vehicle engine cylinder block and head face was conducted. Typically, a conformable gasket is applied to provide sealing between the block surface and the head surface, thereby preventing leakage from or into the joined objects while under compression, which is shown in Fig. 14. The engine block surface and head surface belong to the B12 series engine from an automobile company, and they are assembled by tightening ten bolts. The tighten torque is 60 Nm for each bolt, and it is equal to about a 2 MPa face pressure between the block surface and the head surface. From previous researches and contact mechanics [9,13,14,36], contact pressure is one of the main factors affecting the leakage. It directly affects the distribution of the contact surface, which is related to the surface connectivity, and so, the contact pressure is consistently 2 MPa in the case study condition.

As a major sealing surface, the engine cylinder block surface is finished by high-precision milling. As an example, a measured engine cylinder block surface is shown in Fig. 15. According to the experience from engineers in practice, 30 representative surface regions are chosen to indicate the positions where leakage occurs probably. Each surface region has 900 grids in the size of 30×30, and the sampling interval is 0.2 mm.

Table 1 The results of connectivity parameters

Connectivity class	s_{max}	$\bar{\mu}_\alpha$	Ψ
X_1	2	1.051	0
X_2	1	1.051	0
X_3	2	1.107	0
X_4	2	1.051	0
X_5	1	1.051	0
X_6	2	**1.168**	0
X_7	2	1.051	0
X_8	1	1.162	0

Note: The value in bold means the maximum value of the corresponding column.

Table 2 The results of correlation parameters

Connectivity classes in pairs	*mcd*	*acd*	θ
(X_1, X_2)	2.00	6.71	**1**
(X_1, X_3)	8.00	10.05	3
(X_1, X_4)	13.00	16.03	6
(X_1, X_5)	7.00	14.14	6
(X_1, X_6)	12.00	11.18	**1**
(X_1, X_7)	**1.41**	17.46	8
(X_1, X_8)	**1.41**	21.26	12
(X_2, X_3)	2.00	5.66	**1**
(X_2, X_4)	7.00	10.20	3
(X_2, X_5)	**1.41**	9.43	5
(X_2, X_6)	6.08	13.04	2
(X_2, X_7)	5.00	14.14	7
(X_2, X_8)	3.16	19.72	11
(X_3, X_4)	3.00	6.32	**1**
(X_3, X_5)	**1.41**	4.12	**1**
(X_3, X_6)	2.24	10.30	**1**
(X_3, X_7)	10.77	8.49	2
(X_3, X_8)	9.22	14.32	5
(X_4, X_5)	6.08	**3.61**	**1**
(X_4, X_6)	**1.41**	15.56	5
(X_4, X_7)	15.00	8.00	**1**
(X_4, X_8)	14.00	15.00	5
(X_5, X_6)	5.00	12.04	4
(X_5, X_7)	9.49	5.39	2
(X_5, X_8)	8.06	12.17	5
(X_6, X_7)	14.14	11.40	**1**
(X_6, X_8)	13.00	11.70	2
(X_7, X_8)	**1.41**	7.00	**1**

Note: The values in bold mean the minimum value of the corresponding column.

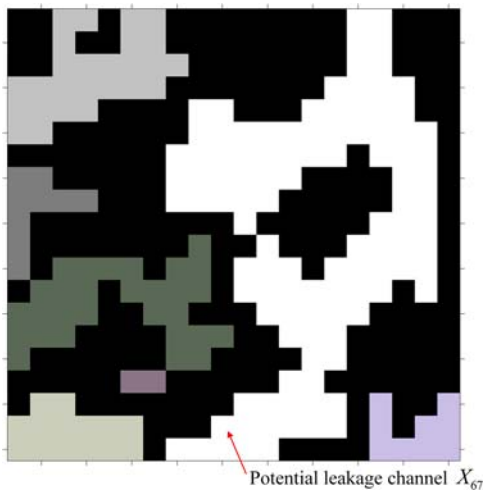

Fig. 13 The potential leakage channel X_{67}

When the leakage parameter *SWvoid* in a surface region goes beyond the threshold *SWvc*, this surface region is namely a leakage surface region or an out of limit (OOL) leakage region. Based on some experimental results in Ref. [21], the threshold *SWvc* satisfied $SWvc \approx 0.300$ in the case study condition. Therefore, the value of *SWvoid* for each surface region is calculated and presented in Table 3, and the OOL leakage regions are found when the corresponding *SWvoid* is greater than 0.3. For a clear visualization, Fig. 16(*a*) illustrates the line chart of *SWvoid*, and the OOL leakage regions are numbered in Fig. 16(*b*).

From these results, it is clear that there are 13 surface regions including region 2, 5, 7, 8, 10, 12, 16, 18, 20, 22, 23, 24, and 26, which are OOL leakage regions. Once the leakage region is found, and the next step is to clarify the leakage channel in these regions. In addition, region 12 has the maximum value of *SWvoid* and region 11 has the minimum value of *SWvoid*. Let the two regions be the representative leakage region and no leakage region, and the corresponding contact surfaces are shown in Fig. 17. Obviously, most part of region 11 are contact, but the contact condition is opposite in region 12 (the black denotes total contact and the white denotes no contact). Hence, there is a need to further analyze region 12 and find out the leakage channel based on the proposed approach in Sec. 3.

In Fig. 18(*a*), the connectivity classes are highlighted in different grayscales and the number of connectivity classes is $n = 6$ in region 12. Here, the grayscales do not mean the height information but mean different connectivity classes. Connectivity parameters and correlation parameters are calculated and presented in Tables 4 and 5.

Obviously, it does not exist $\Psi = 1$, the condition of case 2: $\Psi_2 = 0$ is considered. Then, the size of connectivity is calculated further.

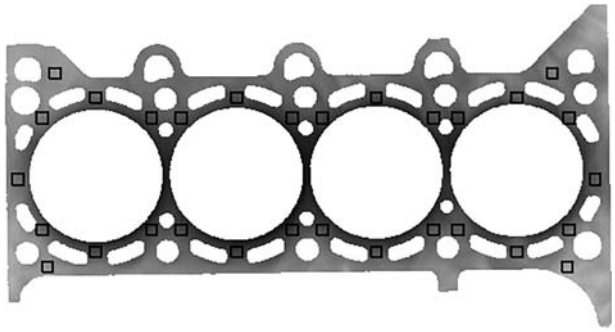

Fig. 15 Thirty surface regions

The four indices are calculated as follows:

$$\begin{cases} \bar{\mu}_{\alpha k_0} = \bar{\mu}_{\alpha 4} = 1.201 \\ mcd_{k_1 k_2} = \{mcd_{15}, mcd_{16}, mcd_{24}\} = 1.41 \\ acd_{k_3 k_4} = \{acd_{56}\} = 7.62 \\ \theta_{k_5 k_6} = \{\theta_{23}, \theta_{34}, \theta_{35}, \theta_{36}, \theta_{46}\} = 1 \end{cases} \tag{40}$$

Finally, the maximum value of connectivity $\bar{\mu}_\alpha(X_k)$ is calculated as follows:

$$\begin{aligned} \bar{\mu}_\alpha(X_k) &= \max\left\{ \begin{matrix} \bar{\mu}_\alpha(X_4), \bar{\mu}_\alpha(X_{15}), \bar{\mu}_\alpha(X_{16}), \bar{\mu}_\alpha(X_{24}), \bar{\mu}_\alpha(X_{56}), \\ \bar{\mu}_\alpha(X_{23}), \bar{\mu}_\alpha(X_{34}), \bar{\mu}_\alpha(X_{35}), \bar{\mu}_\alpha(X_{36}), \bar{\mu}_\alpha(X_{46}) \end{matrix} \right\} \\ &= \bar{\mu}_\alpha(X_{34}) = 1.272 \end{aligned} \tag{41}$$

So the bi-closing connectivity class X_{34} is considered as the potential leak channel of region 12, which is shown in Fig. 18(*b*).

Considering the other 12 OOL leakage regions including region 2, 5, 7, 8, 10, 16, 18, 20, 22, 23, 24, and 26, each surface region is analyzed by the proposed approach and the corresponding leakage

Table 3 The value of *SWvoid* for each surface region

Surface region	*SWvoid*	Surface region	*SWvoid*	Surface region	*SWvoid*
Region 1	0.299	Region 11	0.229	Region 21	0.247
Region 2	**0.317**	Region 12	**0.384**	Region 22	**0.322**
Region 3	0.284	Region 13	0.274	Region 23	**0.353**
Region 4	0.253	Region 14	0.293	Region 24	**0.323**
Region 5	**0.303**	Region 15	0.280	Region 25	0.247
Region 6	0.286	Region 16	**0.367**	Region 26	**0.376**
Region 7	**0.362**	Region 17	0.260	Region 27	0.261
Region 8	**0.307**	Region 18	**0.310**	Region 28	0.282
Region 9	0.237	Region 19	0.298	Region 29	0.271
Region 10	**0.349**	Region 20	**0.314**	Region 30	0.288

Note: The values in bold denote that *SWvoid* goes beyond *SWvc*.

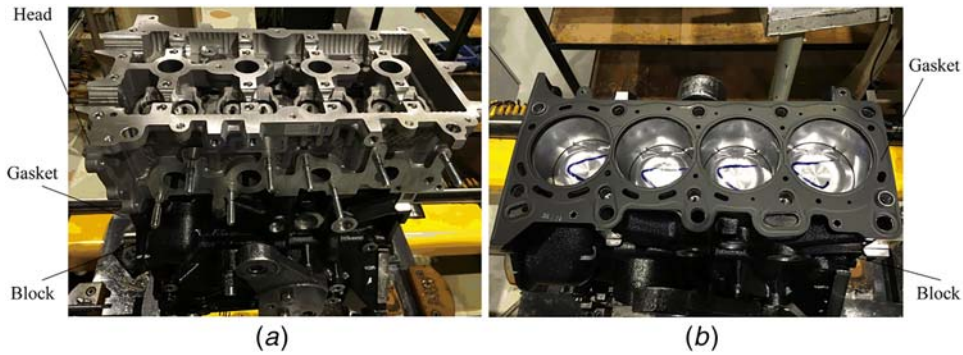

Fig. 14 (*a*) Assembled engine cylinder head and block and (*b*) gasket and block

Table 4 The results of connectivity parameters

Connectivity class	s_{max}	$\bar{\mu}_\alpha$	Ψ
X_1	2	1.168	0
X_2	2	1.078	0
X_3	2	1.107	0
X_4	2	**1.201**	0
X_5	1	1.051	0
X_6	2	1.107	0

Note: The value in bold means the maximum value of the corresponding column.

Table 5 The results of correlation parameters

Connectivity classes in pairs	*mcd*	*acd*	θ
(X_1, X_2)	12.04	21.10	4
(X_1, X_3)	7.00	17.89	2
(X_1, X_4)	11.00	17.00	2
(X_1, X_5)	**1.41**	17.80	6
(X_1, X_6)	**1.41**	25.24	10
(X_2, X_3)	3.00	11.18	**1**
(X_2, X_4)	**1.41**	28.32	12
(X_2, X_5)	10.05	18.87	11
(X_2, X_6)	13.60	24.04	11
(X_3, X_4)	2.00	18.36	**1**
(X_3, X_5)	5.00	7.81	**1**
(X_3, X_6)	9.43	13.15	**1**
(X_4, X_5)	9.00	11.40	2
(X_4, X_6)	13.00	14.56	**1**
(X_5, X_6)	4.47	**7.62**	2

Note: The values in bold mean the minimum value of the corresponding column.

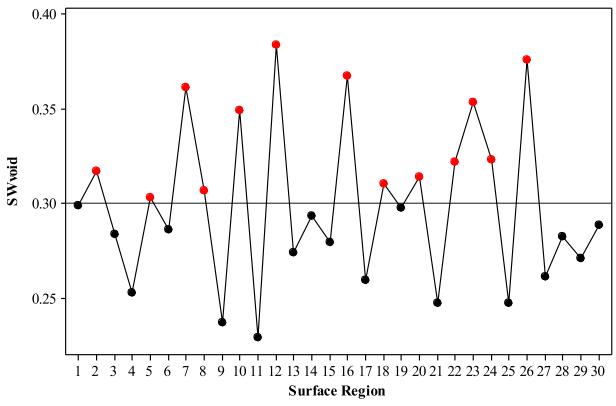

(*a*)

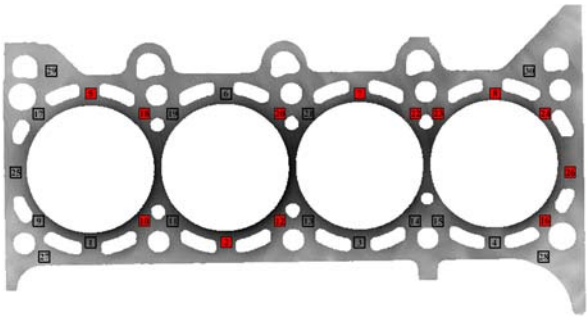

(*b*)

Fig. 16 (*a*) The line chart of *SWvoid* and (*b*) OOL leakage regions

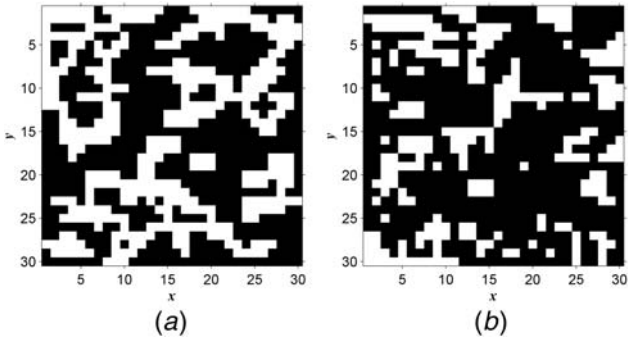

(*a*) (*b*)

Fig. 17 (*a*) The contact surface of region 12 and (*b*) the contact surface of region 11

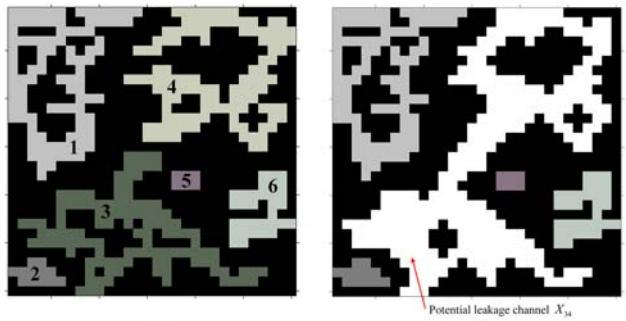

(*a*) (*b*)

Fig. 18 (*a*) Different connectivity classes and (*b*) the leakage channel of region 12

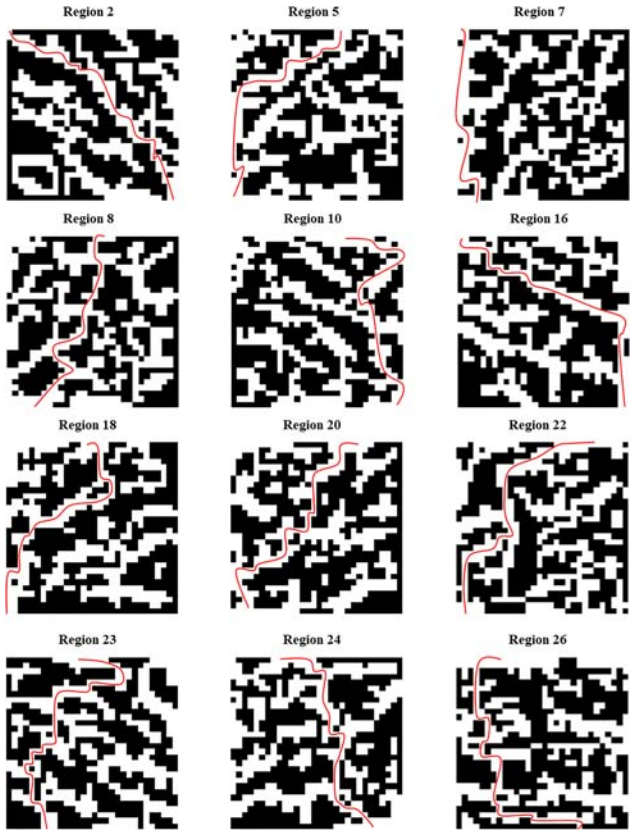

Fig. 19 Leakage channels of OOL surface regions

channel is found. Figure 19 shows all the leakage channels in these leakage surface regions. To demonstrate more clearly, the leakage channels are highlighted by curve lines.

From these experimental results, the proposed leakage channel prediction approach is valid to be accurate and effective, which can provide valuable information for surface topography and static sealing performance. At the same time, the potential leakage channel can reflect the surface irregularities, thereby detecting the machining defects. On the other hand, the problem-oriented leakage prevention measures are adopted before the product entering the next costly machining process. Furthermore, predicting the exact leakage channel also guarantee a qualified surface topography, thereby achieving the functional behavior of the product and decreasing the scrap rate.

5 Conclusions

In this paper, a novel leakage channel prediction approach is proposed based on the surface connectivity. The proposed approach consists of three modules including contact surface generation, leakage parameters definition, and leakage channel prediction. The contact surface that reflects leakage is defined by assembling the virtual gasket surface and waviness surface. Two kinds of leakage parameters including connectivity parameters and correlation parameters are proposed to describe the characteristics of the contact surface. A novel leakage channel prediction algorithm is developed based on the proposed leakage parameters. A leakage index Ψ is built to directly indicate the potential leakage channel of the surface. Experimental results verified the accuracy and effectiveness of the proposed approach, which can provide valuable information for surface topography and static sealing performance.

Furthermore, the topics of surface topography and leakage in static sealing are less studied in the prior research, and the proposed approach in this paper is expected to fill in few gaps in the current research. Following the research phases of leakage, the approach to calculate leak rate based on the 3D surface topography will be explored in the next research topic.

Acknowledgment

This research work was supported by the National Natural Science Foundation of China (Grant Nos. 51535007 and 51775343). We are grateful to the help and experimental support of SAIC GM Wuling Automobile (SGMW) engineers.

References

[1] Flitney, R. K., 2011, *Seals and Sealing Handbook*, Elsevier, Oxford, UK.
[2] Lebeck, A. O., 1981, "Hydrodynamic Lubrication in Wavy Contacting Face Seals—A Two Dimensional Model," ASME J. Lubr. Technol., **103**(4), pp. 578–586.
[3] Robbe-Valloire, F., and Prat, M., 2008, "A Model for Face-Turned Surface Microgeometry. Application to the Analysis of Metallic Static Seals," Wear, **264**(11–12), pp. 980–989.
[4] Aharony, A., and Stauffer, D., 2003, *Introduction to Percolation Theory*, Taylor & Francis, London.
[5] Persson, B. N. J., Albohr, O., Creton, C., and Peveri, V., 2004, "Contact Area between a Viscoelastic Solid and a Hard, Randomly Rough, Substrate," J. Chem. Phys., **120**(18), pp. 8779–8793.
[6] Persson, B. N. J., and Yang, C., 2008, "Theory of the Leak-Rate of Seals," J. Phys. Condens. Matter, **20**(31), p. 315011.
[7] Bottiglione, F., Carbone, G., Mangialardi, L., and Mantriota, G., 2009, "Leakage Mechanism in Flat Seals," J. Appl. Phys., **106**(10), p. 104902.
[8] Bottiglione, F., Carbone, G., and Mantriota, G., 2009, "Fluid Leakage in Seals: An Approach Based on Percolation Theory," Tribol. Int., **42**(5), pp. 731–737.
[9] Lorenz, B., and Persson, B. N. J., 2010, "Leak Rate of Seals: Effective-Medium Theory and Comparison with Experiment," Eur. Phys. J. E, **31**(2), pp. 159–167.
[10] Pérez-Ràfols, F., Larsson, R., and Almqvist, A., 2016, "Modelling of Leakage on Metal-to-Metal Seals," Tribol. Int., **94**, pp. 421–427.
[11] Ledoux, Y., Lasseux, D., Favreliere, H., Samper, S., and Grandjean, J., 2011, "On the Dependence of Static Flat Seal Efficiency to Surface Defects," Int. J. Press. Vessels Piping, **88**(11–12), pp. 518–529.
[12] Marie, C., and Lasseux, D., 2007, "Experimental Leak-Rate Measurement Through a Static Metal Seal," ASME J. Fluids Eng., **129**(6), pp. 799–805.
[13] Lorenz, B., and Persson, B. N. J., 2009, "Leak Rate of Seals: Comparison of Theory With Experiment," Europhys. Lett., **86**(4), p. 44006.
[14] Lorenz, B., and Persson, B. N. J., 2010, "On the Dependence of the Leak Rate of Seals on the Skewness of the Surface Height Probability Distribution," Europhys. Lett., **90**(3), p. 38002.
[15] Vlădescu, S.-C., Putignano, C., Marx, N., Keppens, T., Reddyhoff, T., and Dini, D., 2018, "The Percolation of Liquid Through a Compliant Seal—An Experimental and Theoretical Study," ASME J. Fluids Eng., **141**(3), p. 031101.
[16] Malburg, M. C., 2003, "Surface Profile Analysis for Conformable Interfaces," ASME J. Manuf. Sci. Eng., **125**(3), pp. 624–627.
[17] Liao, Y., Stephenson, D. A., and Ni, J., 2012, "Multiple-Scale Wavelet Decomposition, 3D Surface Feature Exaction and Applications," ASME J. Manuf. Sci. Eng., **134**(1), p. 011005.
[18] Jianjun, S., Chenbo, M., Jianhua, L., and Qiuping, Y., 2018, "A Leakage Channel Model for Sealing Interface of Mechanical Face Seals Based on Percolation Theory," Tribol. Int., **118**, pp. 108–119.
[19] Zhang, F., Liu, J., Ding, X., and Yang, Z., 2016, "An Approach to Calculate Leak Channels and Leak Rates Between Metallic Sealing Surfaces," ASME J. Tribol., **139**(1), p. 011708.
[20] Ren, J., Park, C., and Wang, H., 2017, "Stochastic Modeling and Diagnosis of Leak Areas for Surface Assembly," ASME J. Manuf. Sci. Eng., **140**(4), p. 041011.
[21] Shao, Y., Yin, Y., Du, S., Xia, T., and Xi, L., 2018, "Leakage Monitoring in Static Sealing Interface Based on Three Dimensional Surface Topography Indicator," ASME J. Manuf. Sci. Eng., **140**(10), p. 101003.
[22] Liu, X., Liu, K., Wang, W., and Gui, C., 2009, "Connectivity Characterization of Three-Dimensional Surface Topography Based on Mathematical Morphology," Proc. Inst. Mech. Eng. J J. Eng. Tribol., **223**(J7), pp. 941–947.
[23] Huang, Z., Shih, A. J., and Ni, J., 2006, "Laser Interferometry Hologram Registration for Three-Dimensional Precision Measurements," ASME J. Manuf. Sci. Eng., **128**(4), pp. 1006–1013.
[24] Du, S., and Fei, L., 2015, "Co-Kriging Method for Form Error Estimation Incorporating Condition Variable Measurements," ASME J. Manuf. Sci. Eng., **138**(4), p. 041003.
[25] Du, S., Huang, D., and Wang, H., 2015, "An Adaptive Support Vector Machine-Based Workpiece Surface Classification System Using High-Definition Metrology," IEEE Trans. Instrum. Meas., **64**(10), pp. 2590–2604.
[26] Huang, D., Du, S., Li, G., and Wu, Z., 2017, "A Systematic Approach for Online Minimizing Volume Difference of Multiple Chambers in Machining Processes Based on High-Definition Metrology," ASME J. Manuf. Sci. Eng., **139**(8), p. 081003.
[27] Shao, Y., Du, S., and Xi, L., 2017, "3D Machined Surface Topography Forecasting With Space-Time Multioutput Support Vector Regression Using High Definition Metrology," ASME 2017 International Design Engineering Technical Conferences and Computers and Information in Engineering Conference, Volume 1: 37th Computers and Information in Engineering Conference, Cleveland, OH, Aug. 6–9, p. V001T002A069.
[28] Shao, Y., Wang, K., Du, S., and Xi, L., 2018, "High Definition Metrology Enabled Three Dimensional Discontinuous Surface Filtering by Extended Tetrolet Transform," J. Manuf. Syst., **49**, pp. 75–92.
[29] Wang, M., Shao, Y., Du, S., and Xi, L., 2015, "A Diffusion Filter for Discontinuous Surface Measured by High Definition Metrology," Int. J. Precision Eng. Manuf., **16**(10), pp. 2057–2062.
[30] Wang, M., Xi, L., and Du, S., 2014, "3D Surface Form Error Evaluation Using High Definition Metrology," Precision Eng., **38**(1), pp. 230–236.
[31] Tzafestas, C. S., and Maragos, P., 2002, "Shape Connectivity: Multiscale Analysis and Application to Generalized Granulometries," J. Math. Imaging Vis., **17**(2), pp. 109–129.
[32] Serra, J., 2000, "Connections for Sets and Functions," Fundam. Inform., **41**(1), pp. 147–186.
[33] ISO, 2015, "*Geometrical Product Specifications (GPS)-Filtration Part 1: Overview and Basic Concepts*," International Organization for Standardization, Geneva, Switzerland, Standard No. ISO 16610-1:2015.
[34] ISO, 2015, "*Geometrical Product Specifications (GPS)-Filtration Part 22: Linear Profile Filters: Spline Filter*," International Organization for Standardization, Geneva, Switzerland, Standard No. ISO 16610-22:2015.
[35] ISO, 2015, "Geometrical Product Specifications (GPS)-Filtration Part 40: Morphological Profile Filters: Basic Concepts," International Organization for Standardization, Geneva, Switzerland, Standard No. ISO 16610-40:2015.
[36] Johnson, K. L., 1985, *Contact Mechanics*, Cambridge University Press, New York.
[37] Lou, S., Jiang, X. Q., Bills, P. J., and Scott, P. J., 2013, "Defining True Tribological Contact Through Application of the Morphological Method to Surface Topography," Tribol. Lett., **50**(2), pp. 185–193.